ADVANCED MATERIALS

Supporting Information

for *Adv. Mater.*, DOI: 10.1002/adma.201700463

A Broadband Fluorographene Photodetector

Sichao Du, Wei Lu, Ayaz Ali, Pei Zhao, Khurram Shehzad, Hongwei Guo, Lingling Ma, Xuemei Liu, Xiaodong Pi, Peng Wang, Hehai Fang, Zhen Xu, Chao Gao, Yaping Dan, Pingheng Tan, Hongtao Wang, Cheng-Te Lin, Jianyi Yang, Shurong Dong, Zhiyuan Cheng, Erping Li, Wenyan Yin, Jikui Luo, Bin Yu, Tawfique Hasan, Yang Xu, Weida Hu,* and Xiangfeng Duan*

Supporting Information

Title Broadband Fluorographene Photodetector

Sichao Du, Wei Lu, Ayaz Ali Hakro, Pei Zhao, Khurram Shehzad, Hongwei Guo, Lingling Ma, Xuemei Liu, Xiaodong Pi, Peng Wang, Hehai Fang, Zhen Xu, Chao Gao, Yaping Dan, Pingheng Tan, Hongtao Wang, Cheng-Te Lin, Jianyi Yang, Shurong Dong, Zhiyuan Cheng, Erping Li, Wenyan Yin, Jikui Luo, Bin Yu, Tawfique Hasan, Yang Xu, Weida Hu,* Xiangfeng Duan*

Single crystal multi-layer graphene has been grown by CVD with controlled number of layers and size, where the first layer grows on top and covers other layers as an inverse pyramid structure.[1] The number of layers at a particular point can be identified by the variation of color contrast in the optical micrograph as shown in Figure S1 a. More accurately, the number of layers is also confirmed by the intensity ratio of the Raman *G* to *2D* mode. Figure S1 e is the Raman spectra of the multi-layer graphene. The *G* peak near 1580 cm^{-1} is referred to E_{2g}-symmetry phonons at the Brillouin zone center. The *2D* peak at 2700 cm^{-1} originates from a two phonons double resonance process, which reflects the band structure of graphene layers. The intensity ratio of the *2D* peak and *G* peak (I_{2D}/I_G) is an effective measure of the number of layers *n* ($1 \leq n \leq 5$).

To prepare the FG/Gr heterostructures, top Gr layers were selectively functionalized with fluorine. Figure S1 b-d show the micrographs of graphene after 20 min, 60 min and 120 min fluorination times. As displayed in Figure S1 f-h and Figure S4 a, the appearance of Raman *D* peak at 1628 cm^{-1}, the change in color of graphene layers, and the appearance of various carbon-fluorine bonds (CF. CF_2, CF_3) are indicative of successful fluorine-functionalization. Raman spectra at the condition (15 W, 20 min) show that only top layer (1L) became FG (indicated by its strong *D* peak at 1628 cm^{-1}), while the underneath layers (2L, 3L, 4L, 5L) are still graphene (indicated by a weak or no *D* peak). It is worth mentioning that we only found fluorine atoms on the topside of the FG. With controlled growth of graphene flakes, we can selectively functionalize the top graphene layer, and control its shape and size.

As displayed in Figure S1 f-h, under condition (15 W, 60 min), a prominent *D* peak in 1L and 2L indicated that both top two layers became FG. At 120 min, the 3L also became FG (see *D* peak intensities of 3L in Figure S1 h). Figure S1 b-d illustrate that the color of graphene changes from a darker shade to a lighter one with decrease of the C/F ratio. It also can be observed that Raman characterization of graphene and FG are similar except the very top layer, where the I_{2D}/I_G ratio of top layer of FG is smaller than that of graphene, which is

due to the decrease of C/F ratio. This difference indicates that top layer graphene is much easier to become FG than the 2nd and 3rd layer.

Figure S4 a illustrates the spectra of the XPS measurements of the graphene and FG. The spectra of FG are fitted with 4 peaks: the sp^2 C-C bond is at 284.6 eV; the sp^3 C-C bond is at 285 eV due to the removal of carbon atoms from the honeycomb lattice; C-F bond and C-F_2 bond are at 289.6 eV and 293.5 eV, respectively, indicating that graphene has been functionalized by fluorine. Only the very top layer became FG, which was verified by the Raman mapping (Figure S4 b).[1] The regions with graphene can be divided in two parts. One part contains different numbers of graphene layers (2LG, 3LG) while the other part is without any underlying graphene (1LG). The Raman spectrum of area 1LG clearly shows the increase of I_D/I_G, which is related to the increasing sp^3 bonds originating from attachment of fluorine atoms to graphene basal plane. I_D/I_G is very weak for 2LG and 3LG, indicating no attachment of fluorine atoms for underlying layers. Similar results were observed for 4LG and 5LG.

When the number of photo-excited electron-hole pairs accumulates at the FG/Gr junction to a certain amount, the electrical field between them offsets/reduces the built-in electrical field of the junction, leading to a saturated separation of the electron-hole pairs and thus a decrease of responsivity. By measuring the photocurrent under different laser irradiances, the corresponding linear dynamic range (LDR) results of our devices are shown in Figure S2 c,d. It can be seen that the FG/Gr devices exhibit a better linear photo-response compared to the Gr/Gr within the entire tested laser irradiance range.

From the equation:[2]

$$\mu_n = \frac{L}{W} C_{ox}^{-1} V_{DS}^{-1} \frac{dI_{DS}}{dV_{GS}} \qquad (4)$$

where the C_{ox} is the oxide capacitance per unit area $C_{ox} = \varepsilon_{ox} / d_{ox}$ and ε_{ox} is the SiO_2 permittivity, we then extract electron field-effect mobility μ_n between 12.4 and 207 $cm^2V^{-1}s^{-1}$.

From the I_{DS} versus V_{GS} of the FG/Gr device at dark condition on logarithmic scale, we can determine the sub-threshold swing from[3] $S = dV_{GS} / d(\log_{10} I_{DS})$, S_{min} = 48 V/decade, much higher than the minimum value of 60 mV/decade for the ideal metal-oxide semiconductor field-effect transistor. Such a high value of S indicates that the oxide capacitance per unit area C_{ox} (322 μF/cm^2) is competing with other capacitances in our case, suggesting strong trapping existing in the system.

The photocurrent as a function of the V_{GS} at 532 nm laser irradiation under different irradiance is exhibited in Figure S3 a. The results can be explained by gate dependent photocurrent with the band bending at FG/Gr junction. Since incident photons excite electrons of FG from valence band to conduction band, electron-hole pairs are formed at FG/Gr interface. When V_{GS} < 45 V, the Fermi level of graphene is heightened, resulting in a downward band bending and an enhanced built-in electric field at FG/Gr junction. Thus more photo-generated holes transfer from FG to graphene, leading to an increase of photocurrent. As the V_{GS} increases, the trapped electrons in the conduction band of FG begin to tunnel through the barrier into the graphene channel, resulting in a decrease of photocurrent. When V_{GS} is high enough (> 65 V), the FG energy band becomes to bend upwards. Thus photo-generated electrons transfer to the graphene channel, leading to an increase of photocurrent.

It is also observed that the Gr/Gr devices show non-negligible responsivity. This can be caused by the minimal PMMA residues and chemical-solvent related contaminations during the transfer process of CVD grown multi-layer graphene, although we already used the modified RCA added wet etching method to fairly remove insoluble inorganic residues and heavy metal contaminants.[4] These remaining residues and contaminations also act as electron-trapping centers, inducing *p*-type doping to graphene. This is also confirmed by the Dirac point measurement (Figure S3 a), where the device under dark condition already exhibits *p*-type doping.

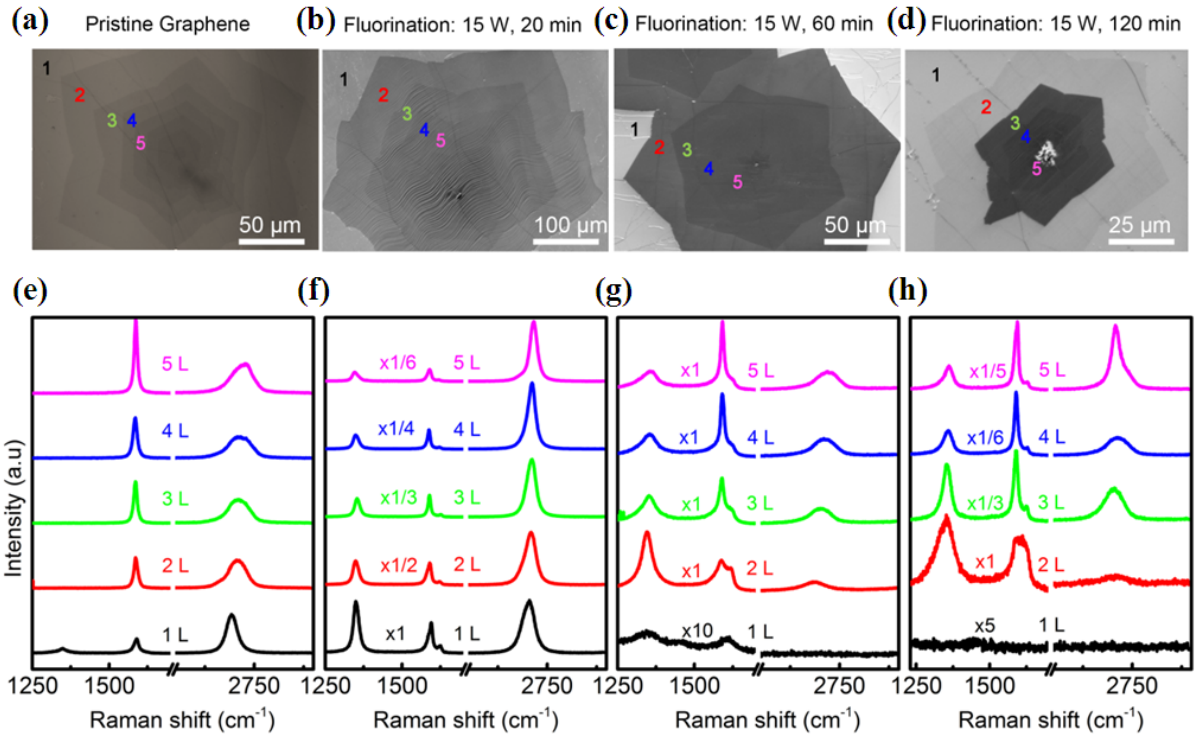

Figure S1. Fluorographene growth and corresponding Raman characterization. a) As grown single-crystal multi-layer CVD-grown graphene transferred on SiO_2 substrate by RCA added wet etching method. The multi-layer graphene after 20 mins (b), 60 mins (c) and 120 mins (d) fluorination with 15 W ICP power. The corresponding Raman spectra (e), (f), (g) and (h) of sample (a), (b), (c) and (d) examined on different sites illustrating one layer (1L) to five layer (5L) structures.

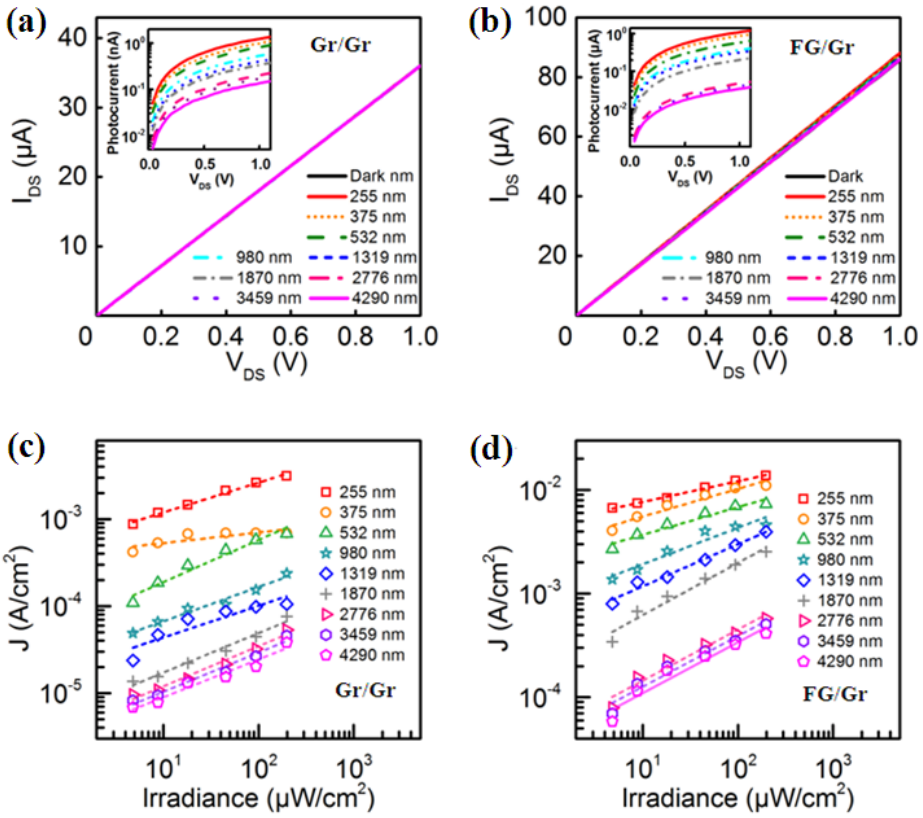

Figure S2. Photo-response results. I_{DS}-V_{DS} curve of the Gr/Gr (a) and FG/Gr (b) devices under dark condition and different wavelength laser illumination. Dynamic range of the photocurrent density of the Gr/Gr (c) and FG/Gr (d) device as a function of the laser irradiance.

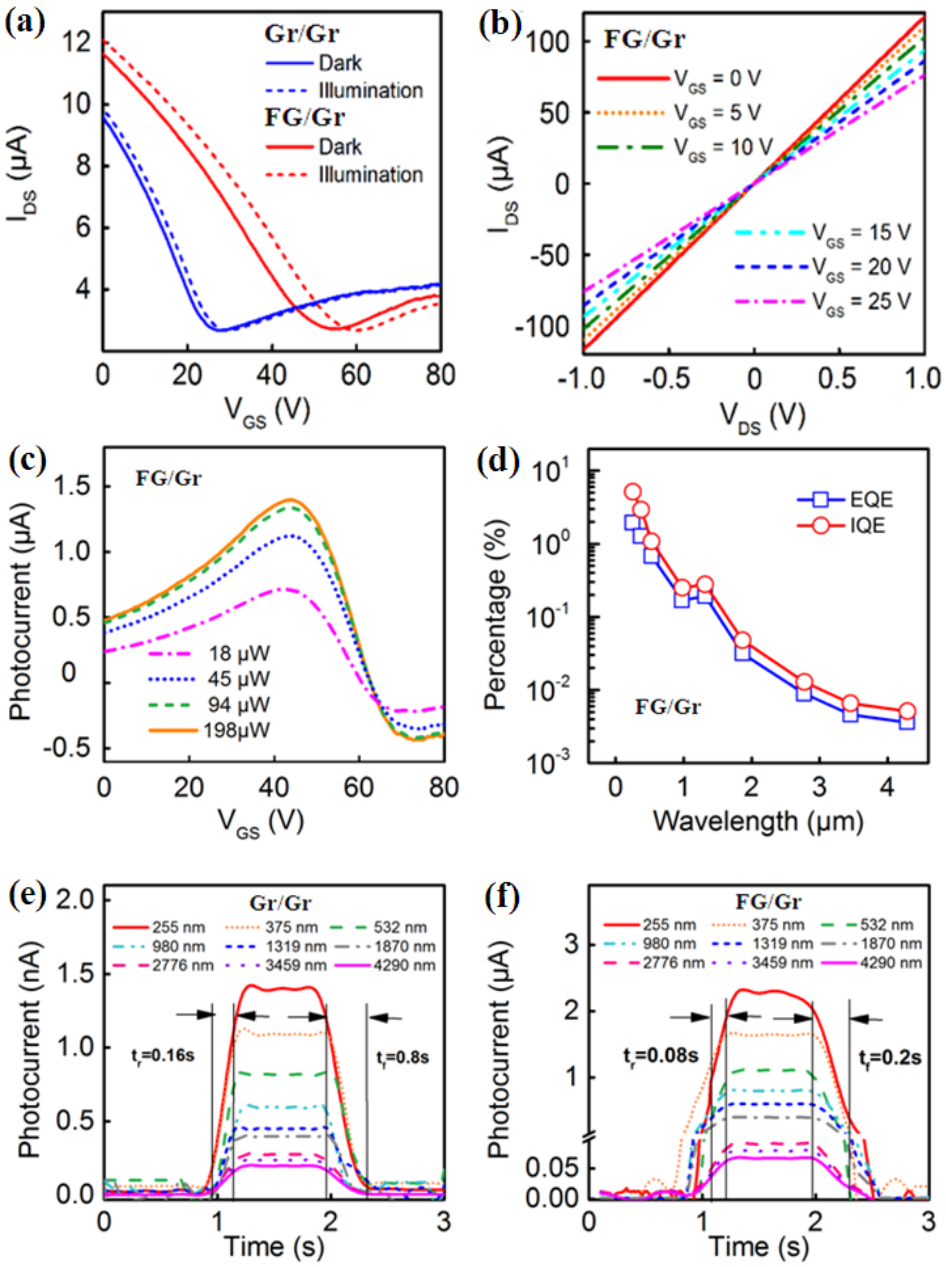

Figure S3. Optoelectronic characteristics. a) I_{DS} as a function of V_{DS} of the Gr/Gr and FG/Gr devices under dark and illumination conditions. b) I_{DS} as a function of V_{DS} at different V_{GS} from 0 to 25 V. c) Photocurrent of the device as a function of V_{GS} with different laser irradiance at 532 nm laser wavelength. d) EQE and IQE as a function of the laser wavelength. Time response of the Gr/Gr (e) and FG/Gr (f) devices in one period, (laser irradiance was 198 μW/cm^2, V_{DS}= 1V, V_{GS}= 28V).

Table S1. List of the key metrics of the related photodetectors in the literature.

Area	Materials	Wavelength [nm]	Responsivity [AW^{-1}]	Response Time [ms]	Ref.
UV	GQDs	254	2.1×10^{-3} @5V	6.4x10@5V	[5]
	ZnO QDs/Gr	325	10^{4} @10^{-3} V	5×10^{3} @10^{-3} V	[6]
	ZnO NRs/Gr	365	1.89×10^{6}	~10^{4} @0.1V	[7]
	ZnOnano rod/rGO	370	22.7	-	[8]
	FG/Gr	255 375	1.4×10^{3}@1V 0.8×10^{3}@1V	80@1V	This work
Visible	Perovskite/Gr	520	10@10^{-2} V	87@0.1V	[9]
	Gr/Ta_2O_5/Gr	532	10^{3} @1V	10@1V	[10]
	FG/Gr	532	0.5×10^{3}@1V	80@1V	This work
	Argon plasma/Gr	535	3.7×10^{-3}@0.01V	9×10^{2}@1V	[11]
	SWNTs/Gr	650	~100@0.5V	~0.1@1.2V	[12]
NIR	PbSnanoplates/Gr	800	2.5×10^{6} @1V	48@1V	[13]
	RGO/P (VDF-TrFE)	800	~2×10^{-5} @9V	~5×10^{4} @9V	[14]
	InGaAs/GaAs	840	0.5@2V	-	[15]
	PbS QDs/Gr	895	10^{4} @1V	3×10^{2} @50mV	[16]
	FG/Gr	980 1319 1870	2.8×10^{2} @1V 1.6×10^{2} @1V 0.7×10^{2} @1V	8.0x10@1V	This work
	InGaAs/InP	1060	5@1V	-	[17]
	GQDs	1470	0.2@20mV	~8×10^{4}@20mV	[18]
	Gr	1550	5 x10^{-4}@4V		[19]
	Bi_2Te_3/Gr	1550	0.2@1V	9.3@1V	[20]
	Black Phosphorus	1700	1.5×10^{-3}@2.5V	0.01@0.1V	[21]
MIR	Gr/Ta_2O_5/Gr	2100	1.9@1V	-	[10]

	Si/Gr	2750	0.13@1.5V	-	[22]
	Gr/Ta_2O_5/Gr	3200	1.1@1V	-	[10]
	FG/Gr	2776 3459 4290	30.8@1V 25.7@1V 21.8@1V	8.0x10@1V	This work
	InAs/InGaAs/InAlAs	4000	34 $x10^{-3}$@2V	-	[23]
	HgCdTe/CdTe	4290	0.01@0V	-	[24]

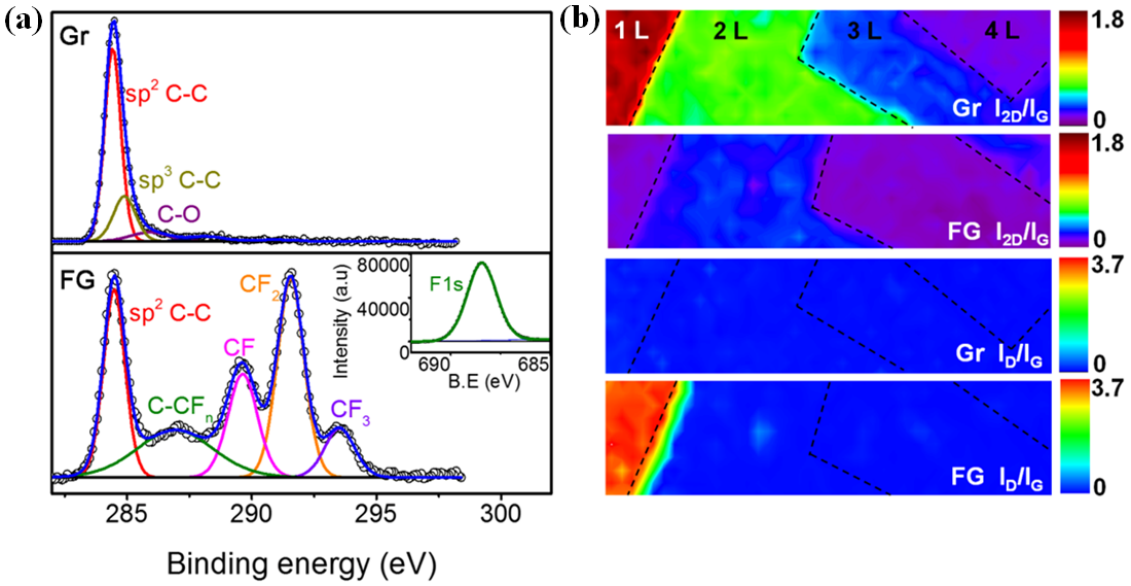

Figure S4. Characterization of fluorine content in fluorographene. a) The XPS results of the single-crystal CVD-grown multi-layer graphene and FG. b) Raman mapping of the graphene and FG/Gr heterostructure. The black dotted lines indicate the boundaries of different layers.

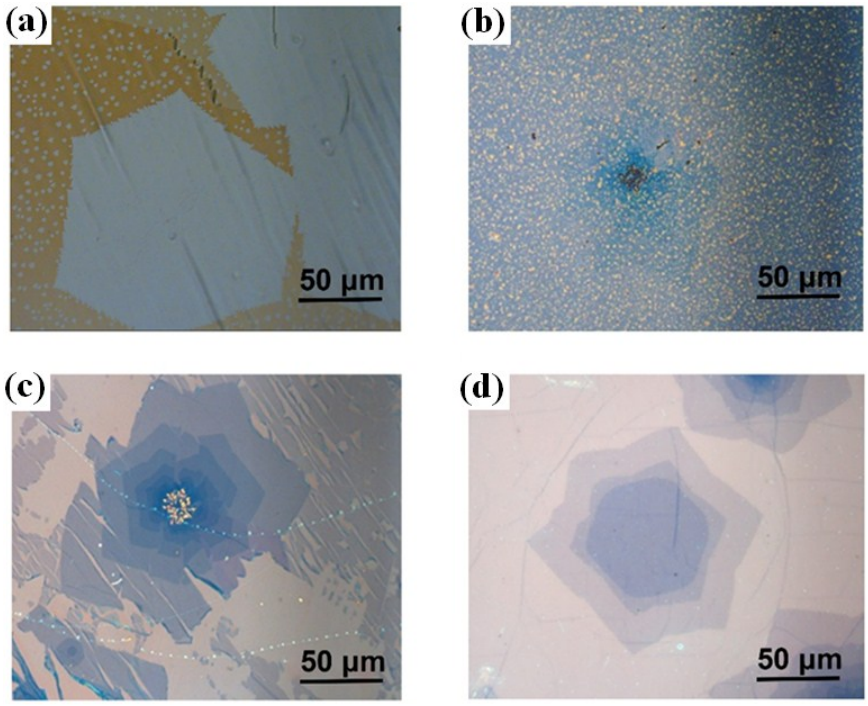

Figure S5. Comparison of different transfer techniques. Graphene on Cu (a) and SiO_2 (b) transferred by wet method, there are many residues. c) The graphene on SiO_2 transferred by bubble method that was broken. d) The graphene on SiO_2 transferred by RCA added wet method, showing clean and high quality graphene films.

[1] Q. Li, H. Chou, J.-H. Zhong, J.-Y. Liu, A. Dolocan, J. Zhang, Y. Zhou, R. S. Ruoff, S. Chen, W. Cai, *Nano Lett.* **2013**, *13*, 486.

[2] M. M. Furchi, D. K. Polyushkin, A. Pospischil, T. Mueller, *Nano Lett.* **2014**, *14*, 6165.

[3] A. Ayari, E. Cobas, O. Ogundadegbe, M. S. Fuhrer, *J. Appl. Phys.* **2007**, *101*, 014507.

[4] X. Liang, B. A. Sperling, I. Calizo, G. Cheng, C. A. Hacker, Q. Zhang, Y. Obeng, K. Yan, H. Peng, Q. Li, X. Zhu, H. Yuan, A. R. Hight Walker, Z. Liu, L.-m. Peng, C. A. Richter, *ACS Nano* **2011**, *5*, 9144.

[5] Q. Zhang, J. Jie, S. Diao, Z. Shao, Q. Zhang, L. Wang, W. Deng, W. Hu, H. Xia, X. Yuan, S.-T. Lee, *ACS Nano* **2015**, *9*, 1561.

[6] W. Guo, S. Xu, Z. Wu, N. Wang, M. M. T. Loy, S. Du, *Small* **2013**, *9*, 3031.

[7] V. Q. Dang, T. Q. Trung, L. T. Duy, B.-Y. Kim, S. Siddiqui, W. Lee, N.-E. Lee, *ACS Appl. Mater. Interfaces* **2015**, *7*, 11032.

[8] H. Chang, Z. Sun, K. Y.-F. Ho, X. Tao, F. Yan, W.-M. Kwok, Z. Zheng, *Nanoscale* **2011**, *3*, 258.

[9] Y. Lee, J. Kwon, E. Hwang, C.-H. Ra, W. J. Yoo, J.-H. Ahn, J. H. Park, J. H. Cho, *Adv. Mater.* **2015**, *27*, 41.

[10] C.-H. Liu, Y.-C. Chang, T. B. Norris, Z. Zhong, *Nat Nano* **2014**, *9*, 273.

[11] K. Thiyagarajan, B. Saravanakumar, S.-J. Kim, *ACS Appl. Mater. Interfaces* **2015**, *7*, 2171.

[12] Y. Liu, F. Wang, X. Wang, X. Wang, E. Flahaut, X. Liu, Y. Li, X. Wang, Y. Xu, Y. Shi, R. Zhang, *Nat Commun* **2015**, *6*, 8589.

[13] Q. Wang, Y. Wen, P. He, L. Yin, Z. Wang, F. Wang, K. Xu, Y. Huang, F. Wang, C. Jiang, J. He, *Adv. Mater.* **2016**, *28*, 6497.

[14] T. Q. Trung, S. Ramasundaram, N.-E. Lee, *Adv. Funct. Mater.* **2015**, *25*, 1745.

[15] F. D. P. Alves, G. Karunasiri, N. Hanson, M. Byloos, H. C. Liu, A. Bezinger, M. Buchanan, *Infrared Physics & Technology* **2007**, *50*, 182.

[16] Z. Sun, Z. Liu, J. Li, G.-a. Tai, S.-P. Lau, F. Yan, *Adv. Mater.* **2012**, *24*, 5878.

[17] H. C. Liu, C. Y. Song, A. Shen, M. Gao, E. Dupont, P. J. Poole, Z. R. Wasilewski, M. Buchanan, P. H. Wilson, B. J. Robinson, D. A. Thompson, Y. Ohno, H. Ohno, *Infrared Physics & Technology* **2001**, *42*, 163.

[18] B. Y. Zhang, T. Liu, B. Meng, X. Li, G. Liang, X. Hu, Q. J. Wang, *Nat Commun* **2013**, *4*, 1811.

[19] F. Xia, T. Mueller, Y.-m. Lin, A. Valdes-Garcia, P. Avouris, *Nat Nano* **2009**, *4*, 839.

[20] H. Qiao, J. Yuan, Z. Xu, C. Chen, S. Lin, Y. Wang, J. Song, Y. Liu, Q. Khan, H. Y. Hoh, C.-X. Pan, S. Li, Q. Bao, *ACS Nano* **2015**, *9*, 1886.

[21] H. Yuan, X. Liu, F. Afshinmanesh, W. Li, G. Xu, J. Sun, B. Lian, A. G. Curto, G. Ye, Y. Hikita, Z. Shen, S.-C. Zhang, X. Chen, M. Brongersma, H. Y. Hwang, Y. Cui, *Nat Nano* **2015**, *10*, 707.

[22] X. Wang, Z. Cheng, K. Xu, H. K. Tsang, J.-B. Xu, *Nat Photon* **2013**, *7*, 888.

[23] S. Tsao, H. Lim, W. Zhang, M. Razeghi, *Appl. Phys. Lett.* **2007**, *90*, 201109.

[24] W. Gawron, P. Martyniuk, A. Kębłowski, K. Kolwas, D. Stępień, J. Piotrowski, P. Madejczyk, M. Pędzińska, A. Rogalski, *Solid·State Electron.* **2016**, *118*, 61.